


# Electron rf Oscillator Based on Self-Excitation of a Talbot-Type Supermode in an Oversized Cavity

Yu. S. Oparina, N. Yu. Peskov, and A.V. Savilov<sup>✉\*</sup>

*Department of Plasma Physics and High-Power Electronics, Institute of Applied Physics of the Russian Academy of Sciences, 46 Ulyanov St., Nizhny Novgorod 603950, Russia*

 (Received 28 May 2019; revised manuscript received 17 September 2019; published 30 October 2019)

We propose the concept of selective excitation of a terahertz operating wave in a high-power electron maser with an oversized microwave system fed by a high-current relativistic electron beam. This concept is based on excitation of a supermode formed by a fixed set of transverse modes, rather than a fixed transverse mode of the operating cavity. A possible approach to form a high- $Q$  supermode inside a simple cavity is the use of the Talbot effect, namely, periodic reproduction of the transverse structure of a multimode wave field in an oversized waveguide.

DOI: [10.1103/PhysRevApplied.12.044070](https://doi.org/10.1103/PhysRevApplied.12.044070)

## I. INTRODUCTION

Currently, there is growing interest in the creation of rf sources operating in the terahertz (THz) and subterahertz frequency range with a high power of the output radiation, as well as in the use of such sources in various applications. Powerful THz sources are required, for instance, for heating and current drive or diagnostic systems of fusion installations of the next generation, such as DEMO [1,2]. One can also mention many actively developing areas, such as high-gradient THz acceleration [3–5], sub-THz wave undulators for short-wavelength free-electron lasers [6–8], and various plasma physics applications [9–11].

A natural way to generate powerful coherent microwave radiation is the use of a powerful high-current relativistic electron beam. However, the problem is that relativistic electron masers [12] (cyclotron resonance masers [13–17], free-electron masers [18–21], Cherenkov and Smith-Purcell devices [22–25]) operating in the millimeter (mm) wavelength range are based typically on excitation of a one chosen far-from-cutoff transverse mode of the operating cavity (waveguide). Moreover, as a rule, this is the lowest possible transverse mode because of the problem of mode selection. Application of this approach to sub-THz and THz waves encounters natural difficulties. Evidently, the operating waveguide in this case should be oversized; this means that the characteristic transverse size should be much greater than that of the operating wavelength. This is necessary for a number of reasons, namely, transportation of the relativistic high-current beam, the problem of breakdown of the field of high-power radiation inside the cavity, ohmic heating of the cavity walls, etc.

In this situation, it is difficult to ensure selective excitation of a definite transverse mode. First, several transverse modes are close to the resonance with electrons in an oversized system. This makes it difficult to provide a single-wave character of the electron-wave interaction [26–29]. The second problem is the difficulty in providing selective single-mode feedback in an oversized system. This is important, especially in auto-oscillators based on excitation of a forward wave with the Doppler-upshifted frequency (that is, a natural scheme for high-frequency masers). A typical configuration of the electron-wave interaction region in such an auto-oscillator is a piece of a waveguide terminated at the input and output ends by two mirrors, which provide feedback, for instance, Bragg-type mirrors can be used to provide effective reflection of far-from-cutoff waves [30] [Fig. 1(a)]. However, if the operating waveguide is oversized, it is difficult to provide selective single-mode reflections from the ends for a far-from-cutoff operating transverse mode [31,32]. In this situation, special methods for selection of the operating mode of the radiated sub-THz wave should be used; one can mention here excitation surface waves in spatially developed waveguides with the distributed 2D feedback [33, 34], the use of two-wave effects (including frequency multiplication) [16,35–38], providing spontaneous character of the THz radiation from specially prepared short electron bunches [39–41], etc. Naturally, we also mention the best-developed solution of the problem described above; this is selective excitation of very-high-order near-cutoff transverse modes in powerful sub-THz cyclotron masers (gyrotrons), operating either at the fundamental resonance [42,43] or at high cyclotron harmonics [44,45]. However, this approach has natural limitations on the generated power.

\*savilov@appl.sci-nnov.ru

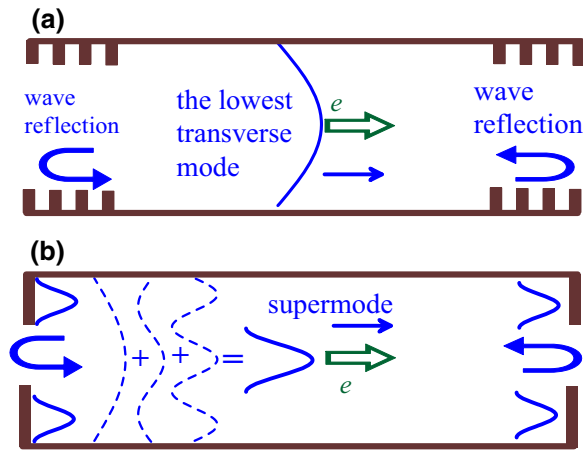


FIG. 1. (a) Traditional scheme of excitation of a far-from-cutoff traveling wave in the cavity formed by a piece of waveguide with two input and output mirrors (Bragg-type mirrors are shown as an example). (b) Excitation of a supermode formed by a set of several transverse modes.

Here, we propose a different concept of selective excitation of a THz operating wave in a high-power relativistic electron maser with an oversized microwave system fed by a high-current relativistic electron beam. Our basic idea is to give up working in a fixed transverse mode. Instead, we propose to work in a supermode, which is formed by a fixed spectrum of several transverse modes of an oversized waveguide [Fig. 1(b)]. The spectrum of the partial transverse modes is determined by both electronic and electrodynamic factors. First, effective interaction between the supermode formed by these partial modes and the electron beam should be provided. This means that, in the middle part of the waveguide, the supermode field should have a maximum at the point of injection of the electron beam into the transverse cross section of the waveguide. Second, the supermode should possess a high  $Q$  factor. Therefore, at the input and output ends of the waveguide, the transverse structure of the supermode field should be very specific, namely, the field should be present only close to the mirrors, to provide almost complete reflection of the supermode back to the cavity [Fig. 1(b)].

In Sec. II, we describe a simple approach, which is based on the use of the Talbot effect [46], namely, periodic reproduction of the transverse structure of a multimode wave field in an oversized waveguide. This effect is widely used in various microwave schemes of electron masers and accelerators [47–50]. We propose to use this approach to fix a high- $Q$  operating supermode in a simple microwave system, consisting of a waveguide terminated by two simple mirrors [Fig. 1(b)]. Section III describes a multimode set of self-consistent equations of the electron-wave interaction, which is valid for a wide class of electron masers (free-electron masers, cyclotron masers, Cherenkov and Smith-Purcell devices). On the basis of this formalism, in

Sec. IV, we demonstrate the possibility of selective self-excitation of the supermode. The “proper” transverse-axial structure of the high- $Q$  supermode is formed at the small-signal stage of the gain guiding during several trips of the wave over the cavity. In fact, the effect described in this paper (formation of a high- $Q$  supermode by a set of several partial transverse modes) is analogous to the effect of mode locking known in the physics of quantum lasers [51]. In Sec. V, the possibility for the realization of a relativistic high-current THz-frequency-range free-electron maser (FEM) oscillator is considered as an example of the use of the approach proposed in this paper.

## II. HIGH- $Q$ TALBOT-LIKE SUPERMODE OF A PLANAR 2D CAVITY

Here, we consider a simple 2D model of the microwave system of an electron rf oscillator in the form of a planar waveguide [Fig. 2(a)] terminated by two mirrors at the input and the output [they are shown in Fig. 2(a) schematically]. We assume that the system is homogeneous along the  $y$  direction; this implies that the waveguide fields are independent of the  $y$  coordinate. We assume also that the operating electron beam interacts only with the waveguide modes possessing the  $y$  component of the electric field. In the particular case of a FEM, this means that the planar undulator of this maser creates the  $x$  component of the periodic magnetic field and, therefore, electrons oscillate in this undulator along the  $y$  coordinate [Fig. 2(a)]. It should be emphasized that such a simple model is chosen only to demonstrate the basic physical effects within a relatively simple formalism. These effects will obviously not disappear when moving to more realistic 3D models of the electron-wave interaction.

We consider a wave field formed by all transverse modes of this system at a fixed frequency. The operating  $y$  component of this field is represented as,

$$\mathbf{E} = \sum_n \mathbf{E}_n = \mathbf{y}_0 \text{Re} \sum_n E_n(z) f_n(x) \exp(i\omega t - ih_n z). \quad (1)$$

Here,  $n$  is the transverse mode number,  $f_n(x) = \sin(k_{\perp,n}x)$  describes the transverse structure of the wave field,  $h_n = \sqrt{k^2 - k_{\perp,n}^2}$  is the axial wave number,  $k = \omega/c = 2\pi/\lambda$ , and  $k_{\perp,n} = \pi n/D$  is the transverse wave number. Generally speaking, the complex amplitudes of the modes,  $E_n(z)$ , depend on the axial coordinate due to amplification of the wave by the operating electron beam.

The condition  $k_{\perp,n} < k$  determines the number of transverse modes involved in the formation of the wave field,

$$n_{\max} = \frac{2D}{\lambda} = 2\hat{D}. \quad (2)$$

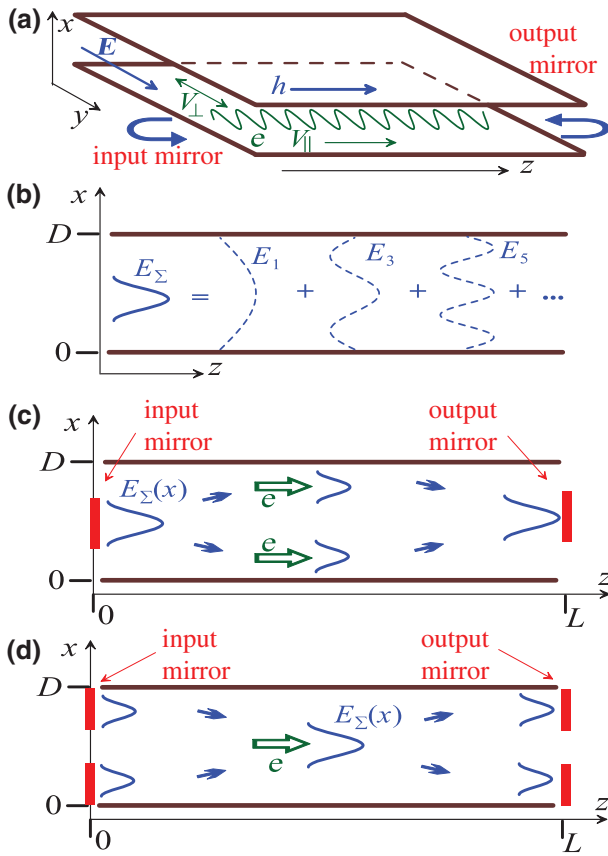


FIG. 2. (a) Schematic of the 2D model of the system (planar waveguide with wave reflection at the input and output ends). (b) Supermode as a wave packet formed by several partial transverse modes. (c),(d) Two variants of Talbot-type supermodes in different cavities.

Here, we introduce the normalized transverse size of the waveguide,  $\hat{D} = D/\lambda$ . In fact, this is the factor of the transverse oversizing of the microwave system. In this paper, we consider the situation of a highly oversized system,  $\hat{D} \gg 1$ . Most of the modes in this situation are very far from the cutoff,  $k_{\perp,n} \ll k$ , and their axial wave numbers can be approximated with high accuracy,

$$h_n \approx k - \frac{k_{\perp,n}^2}{2k} = k - \frac{\pi \lambda n^2}{4D^2}.$$

Within the cold approximation, the phase incursion of the mode during its trip along the waveguide of length  $L$  is equal to

$$\phi_n = h_n L \approx kL - \frac{\pi n^2}{4} \times \frac{\lambda L}{D^2}. \quad (3)$$

Let us consider any symmetrical transverse distribution of the wave field,  $E(x) = E(D-x)$ , which is formed by modes with odd indices,  $n = 2n' - 1$  [Fig. 2(b)]. For these

modes,

$$\phi_n \approx kL - \frac{\pi}{4} \times \frac{\lambda L}{D^2} - \pi n'(n' - 1) \times \frac{\lambda L}{D^2}.$$

Therefore, any symmetrical transverse distribution of the wave field is reproduced in the waveguide,

$$E(x, z + L) = E(x, z), \quad (4)$$

with a period described by

$$L = \frac{D^2}{\lambda}. \quad (5)$$

This phenomenon of repetition of the transverse wave structure is well known in the literature as the Talbot effect [46–49].

We propose to use the Talbot effect as a way to create an oversized microwave system of an electron maser that provides a high  $Q$  factor for a supermode forming several transverse modes [Fig. 2(b)]. Let us imagine that the field of this supermode,  $E_{\Sigma}(x)$ , is concentrated only at the input of the cavity in quite a narrow section close to the center of the waveguide cross section [Fig. 2(c)]. If the length of the waveguide satisfies Eq. (5), then these transverse profiles of the total wave field,  $E_{\Sigma}(x)$ , are reproduced at the output. This wave field can be reflected completely by a simple output mirror that has only a metal surface in the region of the nonzero field area of the supermode. The counter-propagation of the reflected wave back to the input mirror is completely analogous to the direct propagation of the supermode. Therefore, the input mirror, which is similar to the output one, completely reflects the counterpropagating wave into the forward wave and closes the feedback circuit.

Thus, a simple cavity [Fig. 2(c)] provides a high  $Q$  factor for any supermode, the electric field of which,  $E_{\Sigma}(x)$ , is concentrated in the region of the mirrors placed in the middle of the input and output transverse cross sections of the cavity. This high- $Q$  supermode is a specific set of transverse waveguide modes [Fig. 2(b)]. Notably, the separate excitation of each of the partial modes included in this set is not possible. Actually, for every partial mode, the mirrors are semitransparent and, accordingly, the resonator provides a low  $Q$  factor.

One more peculiarity of the Talbot effect is multiplication of the wave beam [46–49]. This means that, in the middle of the cavity shown in Fig. 2(c), the transverse distribution of the supermode field,  $E_{\Sigma}(x)$ , represents two wave beams concentrated close to the waveguide walls. Therefore, such a supermode can be excited effectively by two electron beams injected in the regions close to the walls. Therefore, the problem of separation of the electron beam and the input and output mirrors is easily solved. The natural analogue for the cylindrical geometry of the

scheme shown in Fig. 2(c) is a waveguide of the circular cross section and a tubular electron beam; such beams are traditionally used in high-power cyclotron and Cherenkov masers.

Another scheme of a Talbot-type cavity can be formed by “shifting” the scheme shown in Fig. 2(c) along the  $z$  axis by half of the Talbot length,  $L/2$ . In this case, the supermode forms two wave beams at the input and output of the cavity [Fig. 2(d)]. In the middle of the cavity, these two beams are transformed into one beam located in the middle of the cavity cross section. Again, the electron beam injected in the center of the cross section is easily separated from the input and output mirrors placed near the walls of the waveguide.

Naturally, there is a question of how to form the complicated supermodes shown in Figs. 2(c) and 2(d). In Secs. III–V, we show that such supermodes can be excited by electron beams automatically from random initial noises. The “proper” supermode structures shown in Figs. 2(c) and 2(d) are built-up in the self-consistent process of cavity excitation due to their high  $Q$  factor and effective coupling with the electron beams. In fact, the formation of a supermode is a process of synchronization of several partial transverse waveguide modes both by the electron beam and by the feedback system (i.e., by the shape of the input and output mirrors). To some extent, this process is similar to the synchronization of longitudinal modes in optical lasers [51].

### III. EQUATIONS OF EXCITATION OF A TALBOT-LIKE CAVITY SUPERMODE

#### A. Single-mode asymptotic equation of the electron-wave interaction

As a first step, we consider the process of amplification of a single waveguide mode with a fixed frequency. In the model of a 2D planar waveguide (Fig. 2), the transverse component of the electric field of this wave can be represented as,

$$\mathbf{E}_n = \mathbf{y}_0 \text{Re} E_n(z) f_n(x) \exp(i\omega t - ih_n z).$$

For a wide class of electron masers based on inertial electron bunching in the field of the radiated wave (Cherenkov devices, cyclotron masers, free-electron masers), the evolution of particles in the field of the wave can be described by the universal set of Eqs. (6) and (7) [12,51], which are valid in the case of a small change in the electron energy caused by the electron-wave interaction:

$$\frac{d\gamma}{d\zeta} = -f_n(x_e) \text{Re} \chi A_n \exp(i\theta), \quad (6)$$

$$\frac{d\theta}{d\zeta} = \mu(\gamma_0 - \gamma) - \Delta_n. \quad (7)$$

Here,  $\zeta = kz$  is the axial coordinate of the particle normalized to the wave number of the radiated wave  $k = \omega/c$ ,  $\gamma = 1/\sqrt{1 - (v/c)^2}$  is the relativistic Lorentz factor of the particle,  $A_n = eE_n/kmc^2$  is the normalized wave amplitude,  $x_e$  is the transverse coordinate of the electron beam, and  $\theta$  is the slow resonant phase of the particle with respect to the wave. The initial conditions,

$$\gamma(0) = \gamma_0, \quad \theta(0) = \theta_0 \in [0, 2\pi],$$

describe an electron beam with no spread in initial energy and uniformly mixed over initial phases with respect to the wave. The latter means that we consider the induced radiation from a nonbunched electron beam.

As an example, we illustrate the origin of these equations in the case of a free-electron maser. Equation (6) follows from the general equation for the change in the electron energy,

$$mc^2 \frac{d\gamma}{dz} = -\frac{e}{V_{\parallel}} \mathbf{V} \mathbf{E}, \quad (8)$$

where  $V_{\parallel}$  is the axial component of the electron velocity. Radiation is produced due to the work of the wave field under the oscillating transverse component of the electron velocity,  $\mathbf{V}_{\perp} = \mathbf{y}_0 V_{\perp} \cos(h_u z)$ . The product  $\mathbf{V} \times \mathbf{E}$  includes the slow (resonance) term  $\propto \text{Re} A_n \exp(i\theta)$ , where  $\theta = \omega t - hz - h_u z$  is the resonant phase of the particle with respect to the wave; this phase is slow, if the electron-wave resonance condition  $\omega = (h + h_u) V_{\parallel}$ , is fulfilled approximately [Fig. 3(a)]. Thus, Eq. (8) is transformed into Eq. (6), where the electron-wave coupling factor is determined by the oscillatory electron velocity,  $\chi = V_{\perp}/2V_{\parallel}$ . If the change in the electron energy in the process of the electron-wave interaction is small, then the coupling factor can be assumed to be constant. As for Eq. (7), it is obtained by simple differentiation of the phase,

$$\frac{d\theta}{dZ} = \frac{c}{V_{\parallel}} - \frac{h_n + h_u}{k}. \quad (9)$$

If the change in the electron energy is small, then one can present the right-hand part of Eq. (9) in the form of a Taylor series,

$$\frac{c}{V_{\parallel}} \approx \frac{c}{V_{\parallel 0}} + \mu(\gamma_0 - \gamma),$$

where  $\mu = -(d/d\gamma)(c/V_{\parallel}) = (c^3/V_{\parallel}^3 \gamma^3)$ . This leads to Eq. (7), in which  $\Delta_n = [(h_n + h_u)/k] - (c/V_{\parallel 0})$  is the mismatch of the electron-wave resonance [Fig. 3(a)].

Within the simplest approximation of an amplifierlike case, the spatial evolution of the wave amplitude,  $A(Z)$ , in



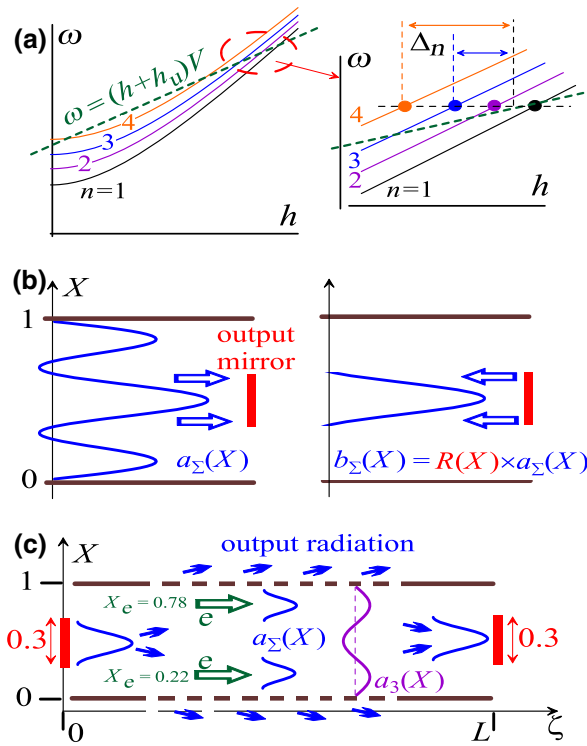


FIG. 3. (a) Dispersion characteristics of different transverse modes and the electron-wave resonance. (b) Reflection of the wave from the output mirror (transverse structures of the forward incident wave packet and the backward reflected wave packet are shown). (c) Schematic of the system studied in simulations (see Sec. IV).

the process of the gain guiding can be described,

$$\frac{dA_n}{d\zeta} = f_n(x_e) \chi G(\exp(-i\theta)). \quad (10)$$

Here,  $\langle \dots \rangle$  denotes averaging over the whole electron ensemble. The excitation factor,  $G$ , can be easily found by means of comparing the integral following from Eqs. (6) and (10),

$$\langle \gamma_0 - \gamma \rangle = \frac{1}{2G} (|A_n|^2 - |A_{n0}|^2),$$

and the energy conservation law,

$$mc^2 \frac{I}{e} \langle \gamma_0 - \gamma \rangle = P_w - P_{w,0}.$$

Since the radiated wave power is proportional to the squared wave amplitude,  $P_w \propto |A_n|^2$ , the excitation factor is determined by the electron beam current,  $G \propto I$ .

Equations (6), (7), and (10) can be transformed into [12,52],

$$\begin{aligned} \frac{du}{d\zeta} &= f_n(x_e) \text{Re} a_n \exp(i\phi), & \frac{d\phi}{d\zeta} &= u, \\ \frac{da_n}{d\zeta} + i\Delta_n a_n &= f_n(x_e) C^3 \langle \exp(-i\phi) \rangle. \end{aligned} \quad (11)$$

Here,  $u = \mu(\gamma_0 - \gamma)$  is the normalized change in the relativistic electron energy,  $\phi = \theta + \Delta\zeta$ ,  $a = \mu \chi A \exp(-i\Delta\zeta)$ , and  $C = (\chi^2 \mu G)^{1/3}$  is the Pierce amplification parameter. Within the framework of this formalism, this is a single parameter that describes the intensity of the electron-wave interaction. In particular, it determines the increment of the wave amplification at the small-signal stage of the gain guiding,

$$a_n \propto \exp(\Gamma \zeta), \quad \Gamma \sim C. \quad (12)$$

Therefore, the product of the Pierce parameter and the normalized cavity length,  $C \times 2\pi L/\lambda$ , is responsible for the degree of axial inhomogeneity of the wave amplitude,  $a(\zeta)$ , that occurs due to gain guiding.

## B. Multimode equations

Notably, the substitutions  $\theta \rightarrow \phi$  and  $A_n \rightarrow a_n$  mean that, instead of the electron phase with respect to the real waveguide wave (with the axial wave number  $h_n(\omega) = \sqrt{k^2 - k_{\perp n}^2}$ ), we introduce the electron phase with respect to an artificial wave that does not exist in this system. The axial wave number,  $h_0$ , of this wave corresponds to the exact electron-wave resonance,

$$\omega = V_{||0}(h_0 + h_u).$$

In other words, now  $h_0$  plays the role of the base wave number, such that

$$\mathbf{E} \propto \mathbf{y}_0 \text{Re} a_n(z) f_n(x) \exp(i\omega t - ih_0 z).$$

This is not important in the case of the interaction of the electron beam with a single waveguide mode. However, this is of principal importance when we generalize the above approach to the case of excitation of a supermode, the field of which is generally a superposition of the fields of all existing transverse modes of the system,

$$\begin{aligned} \mathbf{E} &= \mathbf{y}_0 \sum_n \text{Re} E_n(z) f_n(x) \exp(i\omega t - ih_n z) \\ &= \frac{kmc^2}{e} \mathbf{y}_0 \sum_n \text{Re} a_n(z) f_n(x) \exp(i\omega t - ih_0 z). \end{aligned}$$

Since all components of the supermode have the same base wave number, the total normalized complex amplitude of

the wave field in any cross section of the waveguide is determined as

$$a_{\Sigma}(z, x) = \sum_n a_n(z) f_n(x).$$

In addition, phases of a particle with respect to all transverse modes are the same. Evidently, Eq. (11) is transformed,

$$\begin{aligned} \frac{du}{d\zeta} &= \text{Re} \sum_n f_n(X_e) a_n \exp(i\phi), \quad \frac{d\phi}{d\zeta} = u, \\ \frac{da_n}{d\zeta} + i\Delta_n a_n &= f_n(X_e) C^3 \langle \exp(-i\phi) \rangle - \sigma_n a_n. \end{aligned} \quad (13)$$

Here, the normalized transverse coordinate,  $X = x/D$ , is introduced. At the beginning of the operating cavity,  $\zeta = 0$ , all electrons have the same energies,  $u(0) = 0$ , whereas their initial phases,  $\phi(0)$ , are mixed homogeneously over the interval  $(0, 2\pi)$ .

In the right-hand part of the wave equation in Eq. (13), we introduce the term  $\sigma_n a_n$  to describe the distributed loss of the wave in the waveguide walls. This term may describe both ohmic losses in the walls and, possibly, the output of the radiation from the cavity [see Fig. 3(c) and Sec. IV].

The mismatch of the  $n$ th mode is related to the mismatch of the first mode by the difference between the normalized axial wave numbers of the two waves,  $\hat{h}_n = h_n/k$ ,

$$\Delta_n = \Delta_1 + \hat{h}_n - \hat{h}_1, \quad \hat{h}_n = \sqrt{1 - \left(\frac{n}{2\hat{D}}\right)^2}.$$

In Eq. (13), we assume that the Pierce factor,  $C$ , is the same for all modes, so that the modes differ from each other only by different mismatches of the electron-wave resonance,  $\Delta_n$ , and different fields affecting electrons,  $f_n(x_e) = \sin(\pi n X_e)$ . It should be clarified that, along with this approximation in the framework of this model, we also assume the ideality of the electron beam (no spread in the velocities and in the guiding centers). Also, the transverse structures and dispersion characteristics of all partial modes are found in the approximation of ideal (perfect conductivity) walls of the waveguide.

## B. Simulation of the wave reflections

We model the process of excitation of the supermode of the cavity in time using the trip-by-trip approach. Within this approach, the initial (at the cavity input,  $\zeta = 0$ ) complex amplitude of each partial mode at the current  $N$ th trip,  $a_m(\zeta = 0)|_N$ , is determined by the output amplitudes (at the end of the cavity,  $\zeta = \hat{L} = kL$ ) of all partial

modes amplified by electrons at the previous  $(N-1)$  trip,  $a_m(\zeta = \hat{L})|_{N-1}$ ,

$$a_m(\zeta = 0)|_N = \sum_n K_{m,n} a_n(\zeta = \hat{L})|_{N-1}. \quad (14)$$

Here, the feedback matrix,  $K_{m,n}$ , should describe three successive processes, namely, (i) reflection of the wave from the output reflector, (ii) backward trip of the reflected wave from the output reflector to the input one, and (iii) reflection of this backward wave from the input reflector.

As for the first process, the total wave field that is incident on the output reflector is represented as follows:

$$a_{\Sigma}(X, \zeta = \hat{L}) = \sum_n f_n(X) a_n(\zeta = \hat{L}).$$

The reflected wave field,

$$\begin{aligned} b_{\Sigma}(X, \zeta = \hat{L}) &= R^{\text{out}}(X) a_{\Sigma}(X, \zeta = \hat{L}) \\ &= \sum_n R^{\text{out}}(X) f_n(X) a_n(\zeta = \hat{L}), \end{aligned} \quad (15)$$

is determined by the structure of the output mirror, which is described by the function  $R^{\text{out}}(X)$ ; the latter is equal to one on the metal surface of the mirror and zero in vacuum [Fig. 3(b)]. Naturally, we assume here that the metal surface possesses ideal conductivity.

The backward wave described by Eq. (15) can be decomposed into transverse waveguide modes,

$$b_{\Sigma}(X) = \sum_p f_p(X) b_p, \quad b_p = \frac{\int_0^1 b_{\Sigma}(X) f_p(X) dX}{\int_0^1 f_p^2(X) dX}.$$

This leads to,

$$b_p(\zeta = \hat{L}) = \sum_n R_{p,n}^{\text{out}} a_n(\zeta = \hat{L}). \quad (16)$$

Here,

$$R_{p,n} = \frac{\int_0^1 R(X) f_n(X) f_p(X) dX}{\int_0^1 f_p^2(X) dX}. \quad (17)$$

The backward wave field, which is incident on the front reflector, is taken from Eq. (16), taking into account the different phase incursions for different transverse modes:

$$\begin{aligned} b_{\Sigma}(X, \zeta = 0) &= \sum_p f_p(X) b_p(\zeta = 0), \\ b_p(\zeta = 0) &= \exp(-i\Delta_p \hat{L}) b_p(\zeta = \hat{L}). \end{aligned} \quad (18)$$

The conversion of the backward wave field,  $b_{\Sigma}(X, \zeta = 0)$ , into the forward wave field,  $a_{\Sigma}(X, \zeta = 0)$ , on the input

reflector can be described similarly to Eq. (16). Thus, the feedback loop is closed, and we obtain Eq. (14) from the following feedback matrix:

$$K_{m,n} = \sum_p R_{m,p}^{\text{in}} \exp(-i\Delta_p \hat{L}) R_{p,n}^{\text{out}}. \quad (19)$$

Here, both reflectors are described by the matrices  $R_{m,p}^{\text{in}}$  and  $R_{p,n}^{\text{out}}$ , which are calculated from Eq. (17).

#### IV. INDUCED SELF-EXCITATION OF THE TALBOT-TYPE SUPERMODE BY THE ELECTRON BEAM

In numerical calculations, we study both configurations of the Talbot-type supermode shown in Figs. 2(c) and 2(d). In both cases, the results are very similar, namely, if the starting threshold of the oscillator is exceeded, then the “proper” supermode is excited over a wide range of parameters of the system by the electron beam automatically from random initial noises at the linear (small-signal) stage of the electron-wave interaction. As a result, at the nonlinear stage, the stable generation of the Talbot-type supermode is achieved.

As an example of numerical calculations of the self-excitation of a Talbot-type supermode, here, we describe simulations of the cavity with the input and output mirrors placed in the center of the cross section of the waveguide [Fig. 2(c)]. In these calculations, the transverse size of the waveguide is as large as  $D = 20\lambda$ ; therefore, the waveguide supports 40 transverse modes. According to Eq. (5), in this case, the normalized length of the cavity is

$$\hat{L} = kL = 2\pi \left( \frac{D}{\lambda} \right)^2 \approx 2500.$$

The transverse size of both mirrors amounts to  $0.3D$  [Fig. 3(c)]. Since the Talbot-type supermode forms two wave beams in the middle of the waveguide, we use two symmetrical electron beams to excite this field. The transverse positions of these electron beams are  $x_e = 0.22D$  and  $x_e = 0.78D$  [ $X_e = 0.22$  and  $0.78$ , Fig. 3(c)]. In fact, the electron beams are injected into the first and third maxima of the third partial transverse mode,  $a_3 \propto \sin(3\pi X)$  [Fig. 3(c)]. Therefore, mismatches,  $\Delta_n$ , of the transverse modes are chosen, such that the third transverse mode is closest to the electron-wave resonance.

A significant problem of such Talbot-type systems is that they form supermodes, which are almost completely locked inside the cavity in the build-up regime of rf generation due to the almost complete reflection of their field from the input and output mirrors. To introduce losses of the excited set of the waveguide modes, we use the term  $\sigma_n a_n$  in the right-hand part of the wave equation in Eq. (13). In our model, this term describes both ohmic

losses in the waveguide walls and output of the radiation from the cavity. The latter can be provided either by the use of semitransparent waveguide walls that provide passage of the radiation through the system of holes [as shown in Fig. 3(c)] [53], or by providing scattering of one selected transverse mode into another mode on a periodic Bragg-type structure [54] (which should disrupt the exact implementation of the Talbot effect). It should be recognized that here we do not propose any specific solution to the problem of output of useful radiation from the cavity, and model this process only schematically. More specifically, in the numerical calculations, we introduce the same damping decrements,  $\sigma_n = 0.1/4\hat{L}$ , for all partial transverse modes, which correspond to a loss of approximately 10% of the wave power per round trip through the cavity.

According to numerical calculations, for the parameters of the system described above, the starting value of the Pierce amplification factor is estimated as  $C\hat{L} \approx 1.5$ . In simulations, we consider the case where the electron current does not exceed the starting threshold significantly,  $C\hat{L} = 2$ . According to Eq. (12), this case corresponds to the situation where the effect of gain guiding on the axial structure of amplifying modes is not strong and, therefore, does not disrupt significantly the exact implementation of the Talbot effect. At least, this is true at the steady state of the oscillator operation, whereas the effect of the electron-wave interaction on the effective wave numbers of the amplifying modes is quite noticeable at the small-signal stage of excitation. In particular, this is observed in Fig. 4, which illustrates the trip-by-trip dynamics of excitation of the auto-oscillator. The excitation process starts with small random noises in the electron beam. After the first trip of the wave packet through the cavity, several modes close to the resonance with electrons are excited with different amplitudes and phases [Fig. 4(a)]. The biggest amplitude belongs to the transverse mode with  $n=3$  because this mode is closest to the resonance. As a result, the transverse structure of the wave field in the point before the output mirror is close to the structure of this mode with  $n=3$ . Naturally, the output mirror is almost transparent for this wave field, and about 2/3 of the wave power escapes from the cavity.

However, the situation changes radically during the next several trips of the wave, when the transverse structure of a high- $Q$  supermode is established [Figs. 4(b) and 4(c)]. In the small-signal regime of the electron-wave interaction, we see the supermode formed by a set of mainly five symmetrical transverse modes ( $n = 1, 3, 5, 7, \text{ and } 11$ ). The input mirror reflects this supermode almost perfectly (the power transmission coefficient is under 1%). As for the output mirror, in the small-signal regime, it reflects only about 85% of the power of this supermode back to the cavity. This is due to the effect of the electron-wave interaction on both the spectrum of the excited partial modes and their axial structure. Both of these factors disturb slightly the

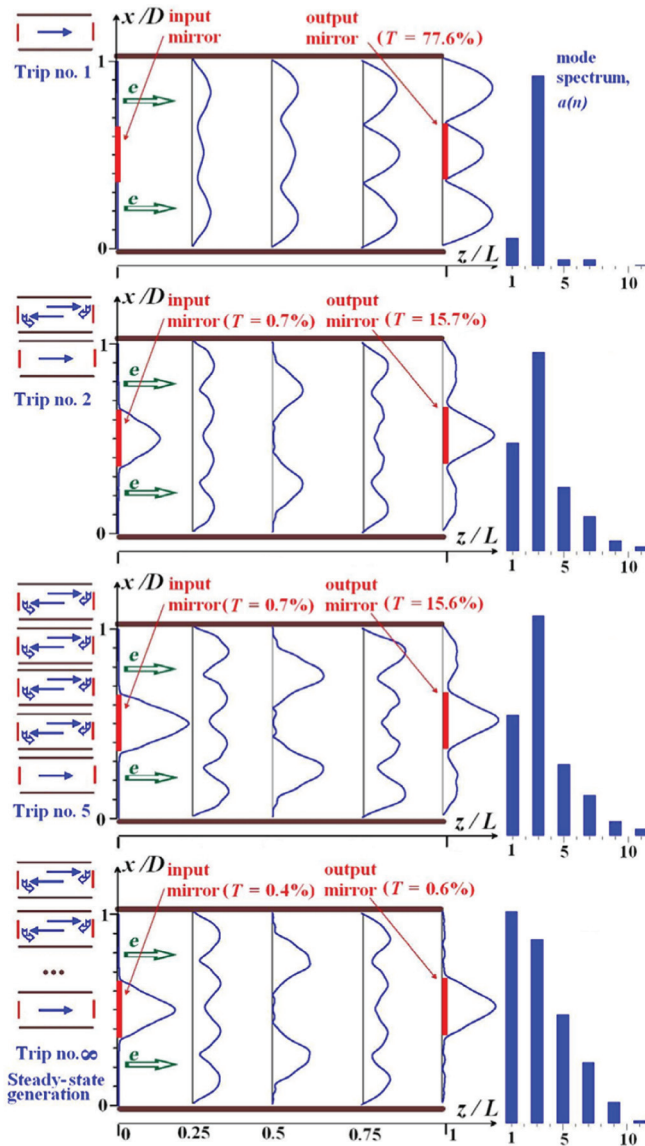


FIG. 4. Evolution of the spatiotemporal structure of the rf wave excited in the Talbot-type cavity. Transverse structures of the wave field in different cross sections of the cavity, and spectra of the excited transverse modes in the small-signal regime of the auto-oscillator excitation after the first (a), second (b), and fifth (c) trips, as well as at the steady-state regime of stable operation (d). Calculated power transmission factors for both mirrors are also shown.

high- $Q$  “cold” structure of the supermode. In other words, the ideal reproduction of the transverse structure of the total field due to the Talbot effect described in Sec. II is slightly disturbed. Specifically, the third transverse mode interacts with the electron beam better than that of the others. This interaction (amplification) results in a significant perturbation of the axial structure of the mode with  $n = 3$  [Fig. 5(a)]. In addition, this leads to the fact that the contribution of this mode to the spectrum of the total supermode field increases [Fig. 4(c)].

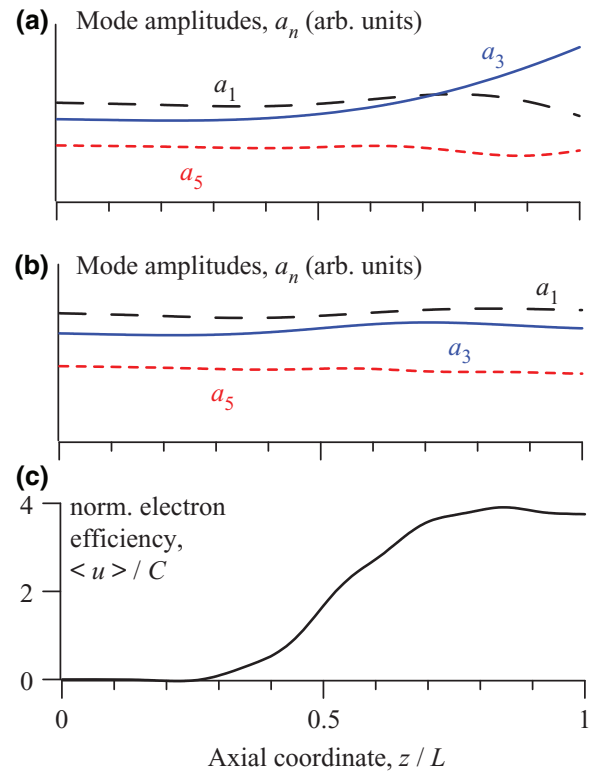


FIG. 5. Axial structures of the partial transverse modes with  $n = 1, 3$ , and  $5$  at the small-signal (a) and nonlinear steady-state (b) stages of the electron-wave interaction, as well as the dependence of the normalized electron efficiency on the axial coordinate at the steady-state stage (c).

The structure of the supermode stays constant during the small-signal stage of the excitation of this auto-oscillator. This stage lasts for several tens of round trips of the wave through the cavity and is then replaced by the nonlinear stage of the stable steady-state generation (Fig. 6). Notably, the normalized electron efficiency in the steady-state regime is in the order of the Pierce factor,  $\langle u \rangle \sim C$  [Fig. 6(a)]. The transition to a nonlinear mode leads to a slight change in the structure of the supermode. This is due to the reduced influence of gain guiding on the axial structure of the resonant transverse modes [compare Figs. 5(a) and 5(b)]. As a result, the Talbot reproduction of the transverse structure of the total supermode field is almost perfect, and the power transmission factor of the output mirror is reduced from 15% (in the small-signal regime) to 0.6%. Thus, in the steady-state regime of rf wave generation, a very high- $Q$  supermode is excited; the total losses of the power of the supermode at the input and output mirrors are about 1% [Fig. 4(c)]. One more result is that, in the steady-state regime, the mode with  $n = 3$  closest to the resonance ceases to be dominant [compare the mode spectra in Figs. 4(c) and 4(d)]. This means that the spectrum of the supermode generated in the steady-state regime is determined by the parameters of the microwave system



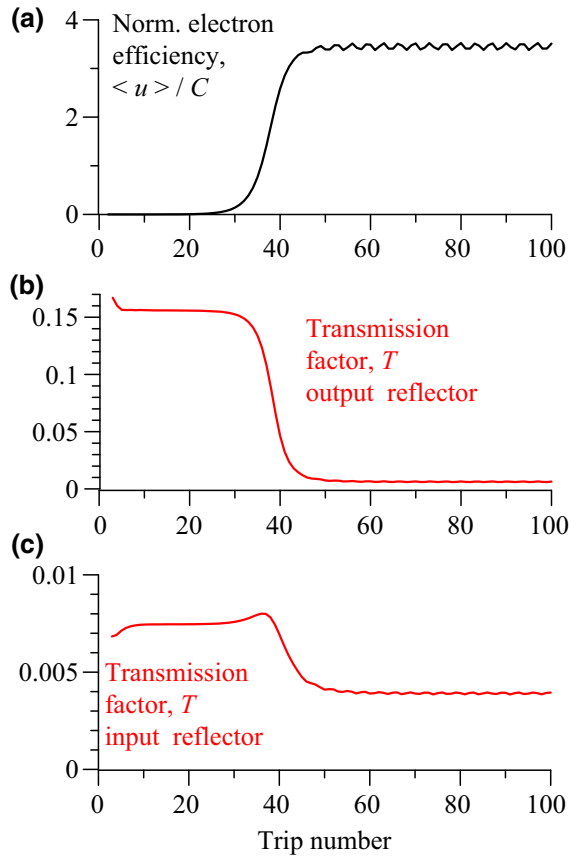


FIG. 6. Dynamics of excitation of the auto-oscillator. Normalized electron efficiency (a), as well as factors of the transmission of the wave power through the output (b) and input (c) mirrors versus the trip number.

(namely, by the size of the input and output mirrors). The predictability of the spectrum of partial transverse modes of the waveguide forming the supermode is an important factor from the point of view of organization of the radiation output from the resonator.

In these numerical calculations, we use two symmetrical electron beams. In this situation, only symmetrical modes ( $n = 1, 3, 5, \dots$ ) are excited. In the case of a small deviation from the symmetry of the electron beams (either in the ratio of currents or in the points of their injection into the cross section of the cavity), a small admixture of asymmetric transverse modes appears. However, this does not lead to a significant change in the structure of the excited supermode.

An important approximation used in the approach described above is the single-frequency character of the process of excitation of the Talbot-type supermode. At the same time, the system of two mirrors provides an effective feedback (a high  $Q$  factor) for this supermode not at a fixed frequency, but within some finite frequency band. Figure 7 shows losses of the power of the excited supermode in the small-signal regimes as functions of the wavelength at

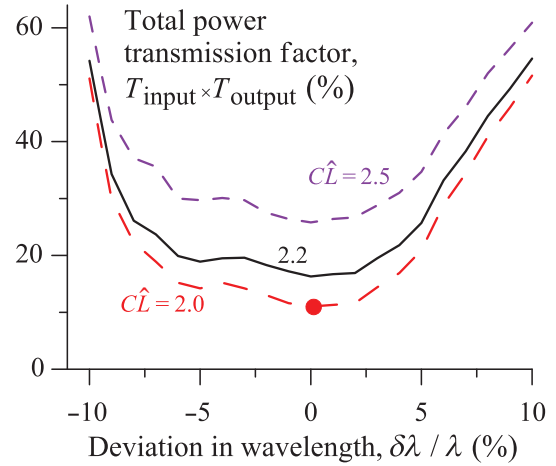


FIG. 7. Total losses of the excited supermode on the input and output mirrors versus the wavelength of the excited wave at different factors of the intensity of the electron-wave interaction,  $C\hat{L}$ .

various values of  $C\hat{L}$ , describing the effect of gain guiding on the axial structures of the resonant partial transverse modes [see Eq. (12)]. More precisely, these are dependences on the deviation,  $\Delta\lambda$ , of the wavelength of the excited supermode from the wavelength,  $\lambda$ , corresponding to the exact execution of the Talbot effect and determined by the geometry of the resonator [see Eq. (5)]. We see that there is a band  $\Delta\lambda/\lambda \sim 7 - 10\%$ , where the losses of the supermode on the mirrors are minimal. Notably, these losses depend on the factor  $C\hat{L}$ . The greater this factor, the greater the disturbance caused the electron-wave interaction in the longitudinal structures of the resonant partial modes and, accordingly, in the performance of the Talbot effect.

Thus, the use of the Talbot-type cavity provides a certain additional selectivity because the Talbot effect occurs over a relatively narrow frequency band [27,55]. At the same time, there exists a multifrequency problem of competition from Talbot-type supermodes with slightly different frequencies, which are within the Talbot frequency band and, therefore, possess relatively high  $Q$  factors. This problem is analogous to the problem of competition between different longitudinal modes in the traditional scheme of an electron auto-oscillator of the simplest Fabry-Perot-type operating cavity (a piece of waveguide with two input and output broadband mirrors) [55–58]. In the latter case, the result of this competition is known, namely, if the operating value of the normalized cavity length,  $C\hat{L}$ , does not exceed significantly the starting threshold, then the longitudinal mode with the biggest small-signal-stage increment wins the competition. This mode is excited faster than that of all its competitors in the small-signal (linear) stage and, accordingly, goes to the nonlinear stage before all the rest, and then suppresses all other competitors. In

our numerical calculations, we consider only excitation of this wave, as we study the case of  $\Delta\lambda = 0$ , where the feedback (and, therefore, the growth increment at the small-signal stage) are maximal. At the same time, the multifrequency theory of oscillators based on excitation of the Talbot-type supermodes should be a subject of future studies.

One more natural question follows. Evidently, many partial transverse modes supported by the operating waveguide (40 modes in our case) can form many high- $Q$  supermodes. The question is which of the supermodes is excited. Our answer is that the structure of the excited supermode is primarily determined by the electron-wave interaction. This fact is illustrated in Fig. 8, which demonstrates the process of excitation of a supermode different from that of the supermodes shown in Fig. 4. The differences between the cases shown in Figs. 4 and 8 are as follows: (i) mode  $n = 5$  (instead of  $n = 3$ ) is close to the electron-wave resonance in Fig. 7, and (ii) slightly different positions of the two electron beams ( $X_e = 0.3/0.7$  instead of  $X_e = 0.22/0.78$ ) are chosen to improve interaction of the beams with the resonant transverse mode  $n = 5$ . The change in the parameters of the electron-wave interaction results in the change in the structure of the excited supermode; in its spectrum, the mode with  $n = 5$  dominates both at the small-signal stage of excitation and in the steady-state regime (Fig. 8). Notably, the  $Q$  factor of this

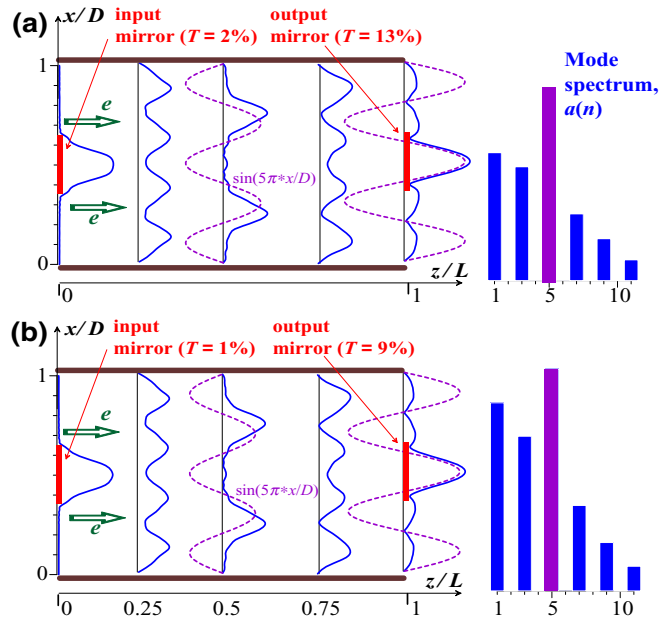


FIG. 8. Evolution of the spatiotemporal structure of the rf wave excited in the Talbot-type cavity when the mode  $n = 5$  is close to the electron-wave resonance. Transverse structures of the wave field in different cross sections of the cavity and spectra of the excited transverse modes in the small-signal regime of the auto-oscillator excitation (a) and in the steady-state regime (b).

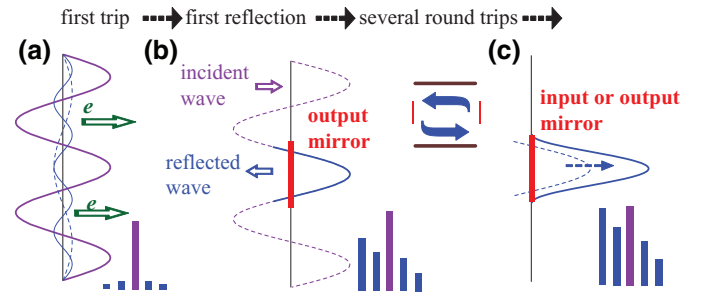


FIG. 9. Scenario for formation of the high- $Q$  Talbot-type supermode. (a) First wave trip through the waveguide before the first reflection leads to amplification of the close-to-resonance partial mode. (b) First reflection of the wave packet: the output mirror “cuts out” its central part. (c) During the next several round trips of the wave packet, the supermode structure is slightly “corrected” by both the electron-wave interaction process and reflections from the input and output mirrors.

supermode is lower than that of the supermode shown in Fig. 4, namely, the power transmission factor for the output mirror is about 10%. Therefore, operation at higher resonant transverse modes can be a way to provide the output of useful radiation from the cavity.

Figure 9 illustrates the scenario of formation of the high- $Q$  Talbot-type supermode. In the first forward trip through the cavity, the initial wave signal is a noise set of several transverse modes; however, the electron beam amplifies the mode that is closest to the resonance with electrons [Fig. 9(a)]. In the process of the first reflection of the wave packet, the output mirror “cuts out” its central part [Fig. 9(b)], which is transmitted to the next trip without distortion due to the Talbot effect. During the next several round trips of the wave packet, the supermode structure is slightly “corrected”; as a result, the transverse structure of the supermode field in the region of the input and output mirrors is located within the mirrors [Fig. 9(c)]. Thus, the process of supermode formation is a combined result of electronic and electrodynamic selection of the “correct” set of transverse modes.

Let us discuss possible parameters for some concrete examples of sub-THz and THz sources based on the use of Talbot-type cavities. Although the formalism used above is appropriate for a wide class of relativistic electronic masers (free-electron masers, cyclotron masers, Cherenkov and Smith-Purcell devices), we consider a free-electron maser, which is probably the most convenient candidate in these frequency ranges. The basic parameters of the system are determined by the factor of the transverse oversizing of the microwave system,  $\hat{D} = D/\lambda$ . According to Eq. (5), the length of a Talbot-type cavity is estimated as

$$L = \lambda \hat{D}^2. \quad (20)$$

If the undulator factor is not too big, then the undulator period is related to the wavelength by

$$\lambda_u \approx \lambda 2\gamma^2. \quad (21)$$

Therefore, the number of undulator periods of the undulator on the length of the electron-wave interaction region is

$$N_u = L/\lambda_u \approx \frac{\hat{D}^2}{2\gamma^2}. \quad (22)$$

If the optimal regime of the electron-wave interaction is provided, then the efficiency is described by [12]

$$\eta \approx 1/N_u. \quad (23)$$

We can consider the situation when the cross section of the system is fixed by the thickness of the operating electron beam. If the undulator period is also fixed, then the radiation wavelength is determined by the electron energy, in accordance with Eq. (21). In this case, the shortening of the wavelength increases the cavity length,  $L \propto 1/\lambda$ , which naturally increases the duration of the excitation process. At the same time, the efficiency decreases,  $\eta \propto \lambda$ . Evidently, these are the most important factors that limit the transverse oversizing of the Talbot-type system.

## V. MODELING OF A 2 THz HIGH-CURRENT FEM OSCILLATOR

As a possible application of the proposed approach, we consider the possibility for the realization of a THz-frequency-range FEM oscillator on the basis of the LIU accelerator being created at the Budker Institute for Nuclear Physics [59,60]. The goal of this work is to provide the formation of a high-current (up to 2 kA) electron beam with electron energy up to 20 MeV and an electron pulse duration of 200–300 ns. The expected thickness of the electron beam is several mm. Therefore, the diameter of the operating waveguide should be at least  $D = 1$  cm. In the case of an operating frequency close to 2 THz, the factor of transverse oversizing,  $D/\lambda$ , is over 60.

In the model, we consider excitation of a cavity in the form of a piece of waveguide with a circular cross section terminated by two mirrors [Fig. 10(a)]. We assume that a helically polarized undulator, together with the axis-encircling electron beam, is used [61]. This means that electrons move along a helix around the axis of the operating waveguide. The basic reason to choose this configuration is an improved selectivity of the system, namely, the axis-encircling electron beam interacts only with  $TE_{1,n}$  and  $TM_{1,n}$  modes, with an azimuthal index equal to one [61]. These “active” modes also have circular polarization, and the direction of their rotation coincides

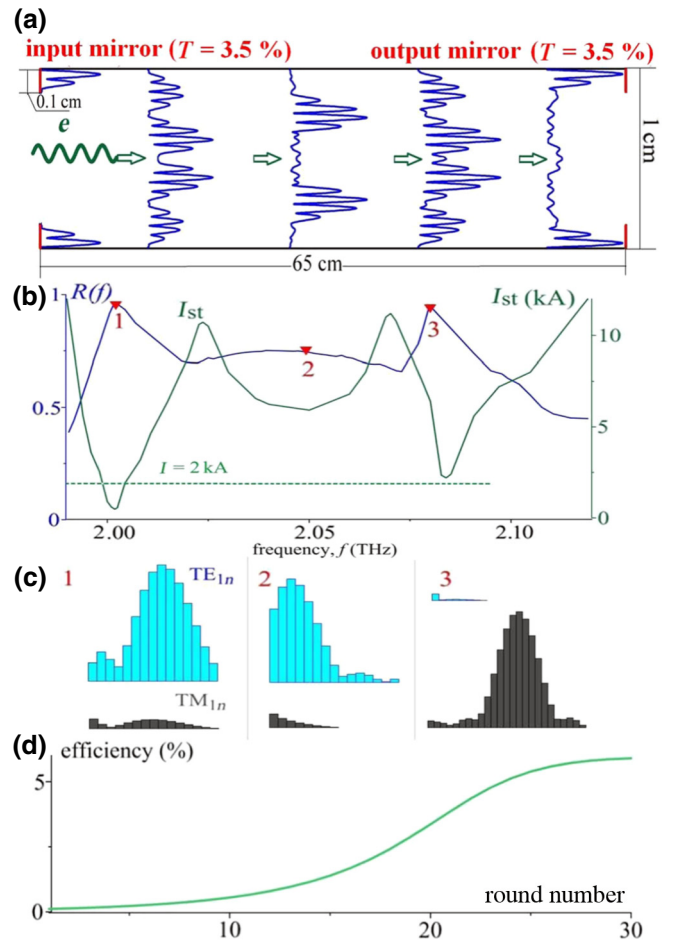


FIG. 10. High-current 2 THz FEM oscillator. (a) Operating cavity and structure of the excited supermode in the steady-state regime [regime “1” in (b); the operating current is 2 kA]. Calculated factors of the transmission of the wave power through the output and input mirrors are also shown. (b) Calculated power reflection coefficient of the input and output mirrors for the high- $Q$  supermode in the “cold” approximation and the starting current of the oscillator versus the frequency. (c) “Cold” amplitude spectra of the supermodes excited in regimes “1”, “2”, and “3” (b). (d) Process of excitation of the FEM oscillator; electron efficiency versus the number of the round trip of the wave through the cavity [regime “1” in (b); the operating current is 2 kA].

with the rotation direction of a circularly polarized field of the undulator. If the input and output mirrors are azimuthally symmetrical, then the description of this system can be limited by consideration of only these transverse modes.

In simulations, we consider the system shown in Fig. 10(a). We use multimode equations of the electron-wave interaction that are analogous to Eq. (13). The only difference is that we should take into account the structures of transverse modes of the circular waveguide describes by Bessel functions (see Appendix). This means, in particular, that the Pierce factors are different for different modes,

namely,

$$C_n = (\chi^2 \mu G_n)^{1/3},$$

where  $\chi \approx K_u/2$  (here,  $K_u = V_\perp/c\gamma$  is the undulator factor),  $\mu \approx \gamma^{-3}$ , and the excitation factor is

$$G_n = \frac{2I}{I_A} \frac{k_{\perp,n}^2}{N_n h_n k}.$$

Here,  $I_A = mc^3/e$  and  $N_n$  is the wave norm. The latter is described in the Appendix, together with the formalism used to describe the reflection of the multimode wave packet from the input and output mirrors in the system with the circular cross section.

In the case of the undulated factor,  $K_u = 0.5$ , and the electron energy, 7 MeV ( $\gamma = 15$ ), the undulator period should be close to 5.5 cm. In the case of  $D = 1$  cm and  $\lambda \approx 0.015$  cm, the Talbot formula leads to  $L \approx D^2/\lambda \approx 65$  cm. Thus, the length of the cavity should be approximately equal to  $N_u = 12$  undulator periods. According to Eq. (23), the estimated electron efficiency in this system should be about 8%.

Accurately, the Talbot effect occurs only in systems with an equidistant spectrum of transverse eigenmodes. In a waveguide with a circular cross section, the mode spectrum is quasi-equidistant; this is true only for sufficiently high transverse modes. Accordingly, the Talbot effect occurs only approximately. Nevertheless, the formation of a high-quality supermode is possible. Curve  $R(f)$  in Fig. 10(b) illustrates the dependence of the diffraction losses of the high- $Q$  supermode on the frequency. This supermode is found in the “cold” approximation, when the electron-wave interaction is absent. Namely, we use Eq. (13), together with the matrix boundary condition that describes the reflection of the multimode wave packet from the input and output mirrors (see Appendix), for a “noise” initial signal in which all partial modes of the system are represented. After several round trips of the wave signal through the cavity, the quasi-stationary structure of the highest-quality supermode is established inside the cavity.

Thus, Fig. 10(b) illustrates the dependence of the power reflection coefficients  $R(f)$  from the input and output mirrors (which are the same in the “cold” approximations) on the frequency. We see that the high- $Q$  supermode exists in a quite narrow frequency band. The mode spectrum of this supermode depends on the frequency. In region 1, this is formed mainly by high-order TE partial modes [Fig. 10(c)]. Notably, due to violation of the quasi-equidistance of the spectrum of these modes, the  $Q$  factor of the supermode turns out to be finite, even without taking into account additional losses in the walls of the system. Namely, the maximum power reflection coefficient of the wave from each of the mirrors is about 95%; therefore, at each round trip of the wave through the cavity,

about 10% of its power is lost. In region 3 in Fig. 10(b), at slightly higher frequencies, we see the high- $Q$  supermode forms basically through the high-order TM modes [Fig. 10(c)]. Interestingly, in the intermediate region of frequencies [region 2 in Fig. 10(b)], we see the supermode formed by relatively low TE and TM modes [Fig. 10(c)]. Since for such modes the equidistance of the spectrum is strongly disturbed, the  $Q$  factor of this supermode is significantly lower, namely, for each mirror  $R \approx 75\%$  and, therefore, about 50% of its power is lost at each round trip of the wave through the cavity.

Curve  $I_{st}(f)$  in Fig. 10(b) illustrates the dependence of the starting current on the frequency. We see that the lowest starting current (approximately 1 kA) is achieved in region 1, corresponding to the TE-type supermode. If the operating current does not exceed 2 kA, then only such a type of supermode can be selectively excited in this system inside a narrow frequency band (less than 0.01 THz). This justifies the use of the single-frequency approximation of the electron-wave interaction in this paper. At higher operating current, generally speaking, we should solve a multifrequency problem to describe competition from different supermodels.

It would seem that the inaccuracy of the equidistant mode spectrum (and, accordingly, the approximate nature of the implementation of the Talbot effect) is a disadvantage of this system. However, this turns out to be a way to solve the problem of ensuring the output of useful radiation from the operating cavity mentioned in Sec. IV. In the case of relatively low operating currents, the effect of the electron-wave interaction on the axial structure of the excited supermode is small. In this case, the same power is carried out from the cavity through the input and output mirrors [for each mirror, the transmission factor is approximately 4%, see Fig. 3(a)]. At higher current and under special conditions, the effect of the electron-wave interaction may provide a significant “hot” perturbation of the Talbot effect, such that a bigger fraction of the output power is carried out through the output mirror. A more detailed description of modeling of this system (including possibilities of “hot” control of the diffraction  $Q$  factor of the operating supermode) will be the subject of future work.

In the case of a close-to-starting electron current,  $I = 2$  kA, the electron efficiency in the steady-state regime amounts to approximately 6% [Fig. 3(d)]. This is close to the estimation mentioned above and means that this regime is close to the optimum of the electron-wave interaction. This corresponds to an output power close to 1 GW at a frequency of 2 THz. The typical duration of the transition process is about 30 round trips of the wave through the cavity, which corresponds to about 100 ns. At higher currents, the duration of the transient process is reduced to ten passes; however, in this case, it would be more correct to solve the multifrequency problem. Notably, the proposed



approach makes it possible, in principle, to provide single-mode self-excitation of an oversize cavity (the transverse dimension is about  $60\lambda$  and the axial dimension is about  $4000\lambda$ ) by an extended electron beam.

## VI. CONCLUSION

We use a very simple model that is as primitive and simplified as possible. First, the model is two dimensional, which, in particular, simplifies greatly the spectrum of the partial transverse modes existing in this system. Second, the simplest pendulumlike asymptotic equations are used to describe the electron-wave interaction; notably, the advantage here is that such equations within a certain approximation are valid for a wide class of relativistic electronic masers (free-electron masers, cyclotron masers, Cherenkov and Smith-Purcell devices). Third, the single-frequency process of excitation of a Talbot-type supermode is considered; here, we consider the frequency corresponding to the biggest growth increment of the wave at the small-signal stage of the electron-wave interaction and suppose that this wave should win in the process of competition at the nonlinear stage of interaction. Finally, the problem of output of useful radiation from the cavity is not considered at all, although this problem turns out to be fundamentally important for this type of system due to the automatic formation of a supermode with a high diffraction  $Q$  factor in the process of self-excitation. All of these problems exist and are important, and their solution should be the subject of future work. Here, we outline only two relatively simple possible ways to solve this problem. They are associated with the violation of the ideal implementation of the Talbot effect. This can be either using a system with a quasi-equidistant spectrum of transverse modes (waveguide with a circular cross section) and/or perturbations of longitudinal structures (phase incursions) of some of the partial modes, forming the normal supermode, due to their interaction with the electron beam.

However, we should state that we deliberately use a model that is as primitive and simplified as possible, as a way towards clear demonstration of the basic physical effects. This is the possibility for selective self-excitation of a supermode formed by a fixed set of transverse modes. This approach can be considered as an alternative (in relation to the traditional excitation of a given transverse mode) concept for the realization of electron masers based on selective excitation of THz operating waves in oversized microwave systems fed by high-current relativistic electron beams. Notably, the proposed system, despite its simplicity, provides both temporal and spatial selectivity. The frequency of the excited Talbot-type supermode is determined simply by the geometry of the operating cavity [namely, the Talbot condition described by Eq. (5)]. Excitation of any partial transverse mode is impossible due to the transparency of the input and output mirrors

for any such mode. The feedback is provided for a special set of partial modes (the supermode) with a zero field in the regions outside the mirrors at the input-output cross sections of the operating waveguide. The concrete spectrum of the supermode is fixed by both the electron-wave resonance and the shape of the input-output mirrors.

## ACKNOWLEDGMENTS

The authors are grateful to Professor A.V. Arzhannikov, Professor G.G. Denisov, and Professor N.S. Ginzburg for useful discussions. The work is supported by the Russian Science Foundation, Project No. 19-12-00212.

## APPENDIX: MODELING OF TRANSFORMATION OF WAVEGUIDE MODES ON THE MIRRORS

We limit our formalism by considering only waves with the “proper” direction of circular polarization (coinciding with the rotation direction of a circularly polarized field of the undulator) and with an azimuthal index equal to one. At a fixed frequency, electric and magnetic fields of a wave packet propagating in the forward direction inside a waveguide with the circular cross section are represented in the cylindrical coordinate system  $(r, \varphi, z)$  as follows,

$$\mathbf{E} = \text{Re}\{\mathbf{E}_\omega(r, z)\exp(i\omega t - i\varphi)\},$$

$$\mathbf{B} = \text{Re}\{\mathbf{B}_\omega(r, z)\exp(i\omega t - i\varphi)\}.$$

The complex wave fields can be decomposed into transverse eigenmodes of the waveguide,

$$\mathbf{E}_\omega(r, z) = \sum_n A_n \mathbf{E}_n(r) \exp(-ih_s z),$$

$$\mathbf{B}_\omega(r, z) = \sum_n A_n \mathbf{B}_n(r) \exp(-ih_s z),$$

where  $h_s = \sqrt{k^2 - k_{\perp,n}^2}$  is the axial wave number,  $k = \omega/c = 2\pi/\lambda$ , and  $k_{\perp,n}$  are the transverse wave numbers of the modes determined further. We take into account that the sum  $\sum_n \dots$  includes both TE and TM modes. For TE<sub>1,s</sub> modes, transverse structures of the field components are described [62]:

$$E_{r,n}(r, \varphi) = i \frac{J_1(k_{\perp,n} r)}{r}, \quad E_{\varphi,n}(r, \varphi) = J_1'(k_{\perp,n} r),$$

$$B_{r,n}(r, \varphi) = \frac{-h_n}{k} E_{\varphi,n}(r, \varphi), \quad B_{\varphi,n}(r, \varphi) = \frac{h_n}{k} E_{r,n}(r, \varphi),$$

$$B_{z,n}(r, \varphi) = -i \frac{k_{\perp,n}^2}{k} J_1(k_{\perp,n} r).$$

Here,  $J_1' = (\partial/\partial r)J_1$ , the transverse wave numbers for these modes are  $k_{\perp,n} = \mu_n'/R_w$ ,  $R_w = D/2$  is the radius of the cross section of the waveguide, and  $\mu_n'$  is the  $n$ th root of

$J'_1(\mu'_n) = 0$ . As for  $\text{TM}_{1,s}$  modes, their transverse structure is described by

$$\begin{aligned} E_{r,n}(r, \varphi) &= J'_1(k_{\perp,n}r), & E_{\varphi,n}(r, \varphi) &= -i \frac{J_1(k_{\perp,n}r)}{r}, \\ E_{z,n}(r, \varphi) &= -i \frac{k_{\perp,n}^2}{h_s} J_1(k_{\perp,n}r), \\ B_{r,n}(r, \varphi) &= \frac{-k}{h_n} E_{\varphi,n}(r, \varphi), & B_{\varphi,n}(r, \varphi) &= \frac{k}{h_n} E_{r,n}(r, \varphi), \end{aligned}$$

where  $k_{\perp,n} = \mu_n/R_w$ , and  $\mu_n$  are the roots of  $J_1(\mu_n) = 0$ .

Let us generalize the formalism describing the reflection of the wave from the mirror (see Sect. III C) for this set of modes. We consider the total wave field incident on the mirror:

$$\vec{\mathbf{E}}_{\omega}(r, z) = \sum_n \vec{A}_n \mathbf{E}_n(r).$$

The reflected field is described by

$$\overleftarrow{\mathbf{E}}_{\omega}(r, z) = R(r) \times \vec{\mathbf{E}}_{\omega}(r, z) = \sum_n \overleftarrow{A}_n \mathbf{E}_n(r) \times R(r).$$

Here,  $R(r)$  describes the mirror; it is equal to one on the metal surface of the mirror and zero in vacuum. The reflected field can be represented as an expansion over waveguide modes:

$$\overleftarrow{\mathbf{E}}_{\omega}(r, z) = \sum_p \overleftarrow{A}_p \mathbf{E}_p(r).$$

Then, we find the matrix,  $R_{p,n}$ , describing the transformation on the mirror of the incident mode,  $\vec{A}_s$ , into the reflected mode,  $\overleftarrow{A}_p$ ,

$$\overleftarrow{A}_p = \sum_n R_{p,n} \vec{A}_n,$$

[see Eq. (16)]. This can be done if we take into account the orthogonality of the waveguide modes,

$$\int [\mathbf{E}_n(r) \times \mathbf{B}_p^*(r)]_z r dr = 0, n \neq p.$$

This easily leads to

$$R_{p,n} = \frac{\int [\mathbf{E}_n \times \mathbf{B}_p^*]_z R(r) r dr}{\int [\mathbf{E}_p \times \mathbf{B}_p^*]_z r dr}.$$

For the transformation of modes of the same type ( $\overrightarrow{\text{TE}}_n \rightarrow \overleftarrow{\text{TE}}_p$  and  $\overrightarrow{\text{TM}}_n \rightarrow \overleftarrow{\text{TM}}_p$ ), this formula is reduced

to [compare with formula (17)]:

$$\begin{aligned} R_{p,n} &= \frac{1}{N_p} \int \left\{ \frac{J_1(k_{\perp,n}r)}{r} \frac{J_1(k_{\perp,p}r)}{r} \right. \\ &\quad \left. + J'_1(k_{\perp,n}r) J'_1(k_{\perp,p}r) \right\} R(r) r dr. \end{aligned}$$

For a pair of modes of different types, the reflection matrix elements are expressed by

$$\begin{aligned} R_{p,n} &= \frac{\pm i}{N_p} \int \left\{ \frac{J_1(k_{\perp,n}r)}{r} J'_1(k_{\perp,p}r) \right. \\ &\quad \left. + J'_1(k_{\perp,n}r) \frac{J_1(k_{\perp,p}r)}{r} \right\} R(r) r dr. \end{aligned}$$

Here,

$$N_p = \int \left\{ \left( \frac{J_1(k_{\perp,p}r)}{r} \right)^2 + (J'_1(k_{\perp,p}r))^2 \right\} r dr$$

is the wave norm, “+” corresponds to the  $\overrightarrow{\text{TE}}_n \rightarrow \overleftarrow{\text{TM}}_p$  transformation, and “−” corresponds to the  $\overrightarrow{\text{TM}}_n \rightarrow \overleftarrow{\text{TE}}_p$  transformation on the mirror.

- 
- [1] R. Wenninger, et al., Advances in the physics basis for the European DEMO design, *Nucl. Fusion* **55**, 063003 (2015).
  - [2] S. Garavaglia, et al., EU DEMO EC system preliminary conceptual design, *Fusion Eng. Des.* **136**, 1173 (2018).
  - [3] E. A. Nanni, W. R. Huang, K.-H. Hong, K. Ravi, A. Fallahi, G. Moriena, R. D. Miller, and F. X. Kärtner, Terahertz-driven linear electron acceleration, *Nat. Commun.* **6**, 8486 (2015).
  - [4] M. C. Hoffmann and J. A. Fülöp, Intense ultrashort terahertz pulses: Generation and applications, *J. Phys. D: Appl. Phys.* **44**, 083001 (2011).
  - [5] M. Fakhari, A. Fallahi, and F. X. Kärtner, THz cavities and injectors for compact electron acceleration using laser-driven THz sources, *Phys. Rev. Accel. Beams* **20**, 041302 (2017).
  - [6] T. M. Tran, B. G. Danly, and J. S. Wurtele, Free-electron lasers with electromagnetic standing wave wigglers, *IEEE J. Quantum Electron.* **23**, 1578 (1987).
  - [7] S. Tantawi, M. Shumail, J. Neilson, G. Bowden, C. Chang, E. Hemsing, and M. Dunning, Experimental Demonstration of a Tunable Microwave Undulator, *Phys. Rev. Lett.* **112**, 164802 (2014).
  - [8] S. V. Kuzikov, A. V. Savilov, and A. A. Vikharev, Flying radio frequency undulator, *Appl. Phys. Lett.* **105**, 033504 (2014).
  - [9] G. S. Nusinovich, P. Sprangle, V. E. Semenov, D. S. Dorozhkina, and M. Yu. Glyavin, On the sensitivity of terahertz gyrotron based systems for remote detection of concealed radioactive materials, *J. Appl. Phys.* **111**, 124912 (2012).

- [10] M. Y. Glyavin, S. V. Golubev, I. V. Izotov, A. G. Litvak, A. G. Luchinin, S. V. Razin, A. V. Sidorov, V. A. Skalyga, and A. V. Vodopyanov, A point-like source of extreme ultraviolet radiation based on a discharge in a non-uniform gas flow, sustained by powerful gyrotron radiation of terahertz frequency band, *Appl. Phys. Lett.* **105**, 4900751 (2014).
- [11] I. S. Abramov, E. D. Gospodchikov, and A. G. Shalashov, Extreme-Ultraviolet Light Source for Lithography Based on an Expanding Jet of Dense Xenon Plasma Supported by Microwaves, *Phys. Rev. Appl.* **10**, 034065 (2018).
- [12] V. L. Bratman, N. S. Ginzburg, and M. I. Petelin, Common properties of free electron lasers, *Opt. Commun.* **30**, 409 (1979).
- [13] A. W. Fliflet, R. B. McCowan, C. A. Sullivan, D. A. Kirkpatrick, S. H. Gold, and W. M. Manheimer, Development of high power CARM oscillators, *Nucl. Inst. Methods Phys. Res. A* **285**, 233 (1989).
- [14] S. Alberti, B. G. Danly, G. Gulotta, E. Giguet, T. Kimura, W. L. Menninger, J. L. Rullier, and R. J. Temkin, Experimental Study of a 28 GHz High-Power Long-Pulse Cyclotron Autoresonance Maser Oscillator, *Phys. Rev. Lett.* **71**, 2018 (1993).
- [15] V. L. Bratman, G. G. Denisov, B. D. Kol'Chugin, S. V. Samsonov, and A. B. Volkov, Experimental Demonstration of High-Efficiency Cyclotron-Autoresonance-Maser Operation, *Phys. Rev. Lett.* **75**, 3102 (1995).
- [16] A. V. Sivilov, V. L. Bratman, A. D. R. Phelps, and S. V. Samsonov, Effective coupling of cyclotron autoresonance maser and "gyrotron" modes on a phase-synchronized electron beam, *Phys. Rev. E* **62**, 4207 (2000).
- [17] K. R. Chu, The electron cyclotron maser, *Rev. Mod. Phys.* **76**, 489 (2004).
- [18] T. S. Chu, F. V. Hartemann, B. G. Danly, and R. J. Temkin, Single-Mode Operation of a Bragg Free-Electron Maser Oscillator, *Phys. Rev. Lett.* **72**, 2391 (1994).
- [19] M. E. Conde and G. Bekefi, Experimental Study of a 33.3-GHz Free-Electron-Laser Amplifier with a Reversed Axial Guide Magnetic Field, *Phys. Rev. Lett.* **67**, 3082 (1991).
- [20] W. H. Urbanus, W. A. Bongers, C. A. J. Van Der Geer, P. Manintveld, J. Plomp, J. Pluygers, A. J. Poelman, P. H. M. Smeets, A. G. A. Verhoeven, V. L. Bratman, G. G. Denisov, A. V. Sivilov, M. Yu. Shmelyov, M. Caplan, A. A. Varfolomeev, S. V. Tolmachev, and S. N. Ivanchenkov, High-power electrostatic free-electron maser as a future source for fusion plasma heating: Experiments in the short-pulse regime, *Phys. Rev. E* **59**, 6058 (1999).
- [21] N. S. Ginzburg, A. A. Kaminsky, A. K. Kaminsky, N. Y. Peskov, S. N. Sedykh, A. P. Sergeev, and A. S. Sergeev, High-Efficiency Single-Mode Free-Electron Maser Oscillator Based on a Bragg Resonator with Step of Phase of Corrugation, *Phys. Rev. Lett.* **84**, 3574 (2000).
- [22] C. Chen, G. Liu, W. Huang, Z. Song, J. Fan, and H. Wang, A repetitive X-band relativistic backward-wave oscillator, *IEEE Trans. Plasma Sci.* **30**, 1108 (2002).
- [23] S. D. Korovin, A. A. Eltchaninov, V. V. Rostov, V. G. Shpak, M. I. Yalandin, N. S. Ginzburg, A. S. Sergeev, and I. V. Zotova, Generation of Cherenkov superradiance pulses with a peak power exceeding the power of the driving short electron beam, *Phys. Rev. E* **74**, 016501 (2006).
- [24] R. Xiao, C. Chen, X. Zhang, and J. Sun, Efficiency enhancement of a high power microwave generator based on a relativistic backward wave oscillator with a resonant reflector, *J. Appl. Phys.* **105**, 053306 (2009).
- [25] V. V. Rostov, I. V. Romanchenko, M. S. Pedos, S. N. Rukin, K. A. Sharypov, V. G. Shpak, S. A. Shunailov, M. R. Ul'Masculov, and M. I. Yalandin, Superradiant K-band Cherenkov oscillator with 2-GW peak power, *Phys. Plasmas* **23**, 093103 (2016).
- [26] V. L. Bratman and A. V. Sivilov, Nonresonant excitation and nonlinear suppression of parasitic transverse modes in free-electron masers, *Int. J. Infrared Millimeter Waves* **14**, 2119 (1993).
- [27] V. L. Bratman and A. V. Sivilov, Simulations of the build-up of transverse and longitudinal structures of the microwave field in the Fusion FEM, *Nucl. Instr. Meth. Phys. Res. A* **407**, 40 (1998).
- [28] D. Zhang, J. Zhang, H. Zhong, and Z. Jin, Analysis of the mode composition of an X-band overmoded O-type Cherenkov high-power microwave oscillator, *Phys. Plasmas* **19**, 103102 (2012).
- [29] R. Xiao, J. Li, X. Bai, X. Zhang, Z. Song, Y. Teng, H. Ye, X. Li, J. Sun, and C. Chen, An overmoded relativistic backward wave oscillator with efficient dual-mode operation, *Appl. Phys. Lett.* **104**, 093505 (2014).
- [30] V. L. Bratman, G. G. Denisov, N. S. Ginzburg, and M. I. Petelin, FEL's with bragg reflection resonators: Cyclotron autoresonance masers versus ubitrons, *IEEE J. Quantum Electron.* **19**, 282 (1983).
- [31] N. S. Ginzburg, A. M. Malkin, N. Y. Peskov, A. S. Sergeev, V. Y. Zaslavsky, K. Kamada, and Y. Soga, Tunable terahertz band planar Bragg reflectors, *Appl. Phys. Lett.* **95**, 043504 (2009).
- [32] S. Ceccuzzi, A. Doria, G. P. Gallerano, G. L. Ravera, I. Spassovsky, N. S. Ginzburg, M. Y. Glyavin, N. Y. Peskov, and A. V. Sivilov, Traditional vs. advanced Bragg reflectors for oversized circular waveguide, *Fusion Eng. Des.* **123**, 477 (2017).
- [33] A. W. Cross, I. V. Konoplev, K. Ronald, A. D. R. Phelps, W. He, C. G. Whyte, N. S. Ginzburg, N. Y. Peskov, and A. S. Sergeev, Experimental studies of two-dimensional coaxial Bragg structures for a high-power free-electron maser, *Appl. Phys. Lett.* **80**, 1517 (2002).
- [34] A. J. MacLachlan, C. W. Robertson, I. V. Konoplev, A. W. Cross, A. D. R. Phelps, and K. Ronald, Resonant Excitation of Volume and Surface Fields on Complex Electrodynamic Surfaces, *Phys. Rev. Appl.* **11**, 034034 (2019).
- [35] V. L. Bratman, A. E. Fedotov, N. G. Kolganov, S. V. Samsonov, and A. V. Sivilov, Effective Co-Generation of Opposite and Forward Waves in Cyclotron-Resonance Masers, *Phys. Rev. Lett.* **85**, 3424 (2000).
- [36] A. V. Sivilov, Cyclotron frequency multiplication in cherenkov backward-wave oscillators, *Phys. Plasmas* **16**, 063103 (2009).
- [37] N. Yu. Peskov, I. V. Bandurkin, A. K. Kaminsky, S. V. Kuzikov, E. A. Perelstein, A. V. Sivilov, S. N. Sedykh, and A. A. Vikharev, High-power free-electron maser operated in a two-mode frequency-multiplying regime, *Phys. Rev. Accel. Beams* **19**, 060704 (2016).

- [38] W. Liu, L. Liang, Q. Jia, L. Wang, and Y. Lu, Multicolor Terahertz Frequency Mixer Using Multibunching of Free-Electron Beams, *Phys. Rev. Appl.* **10**, 034031 (2018).
- [39] F. Ciocci, R. Bartolini, A. Doria, G. P. Gallerano, E. Giovenale, M. F. Kimmitt, G. Messina, and A. Renieri, Operation of a Compact Free-Electron Laser in the Millimeter-Wave Region with a Bunched Electron Beam, *Phys. Rev. Lett.* **70**, 928 (1993).
- [40] N. Balal, I. V. Bandurkin, V. L. Bratman, E. Magory, and A. V. Savilov, Negative-mass mitigation of Coulomb repulsion for terahertz undulator radiation of electron bunches, *Appl. Phys. Lett.* **107**, 163505 (2015).
- [41] Yu. S. Oparina and A. V. Savilov, Spontaneous superradiant sub-THz coherent cyclotron emission from a short dense electron bunch, *Phys. Rev. Accel. Beams* **22**, 030701 (2019).
- [42] G. G. Denisov, A. G. Litvak, V. E. Myasnikov, E. M. Tai, and V. E. Zapevalov, Development in Russia of high-power gyrotrons for fusion, *Nucl. Fusion* **48**, 054007 (2008).
- [43] M. Yu. Glyavin, A. G. Luchinin, G. S. Nusinovich, J. Rodgers, D. G. Kashyn, C. A. Romero-Talamas, and R. Pu, A 670 GHz gyrotron with record power and efficiency, *Appl. Phys. Lett.* **101**, 153503 (2012).
- [44] V. L. Bratman, Yu. K. Kalynov, and V. N. Manuilov, Large-Orbit Gyrotron Operation in the Terahertz Frequency Range, *Phys. Rev. Lett.* **102**, 245101 (2009).
- [45] I. V. Bandurkin, V. L. Bratman, Y. K. Kalynov, I. V. Osharin, and A. V. Savilov, Terahertz large-orbit high-harmonic gyrotrons at IAP RAS: Recent experiments and new designs, *IEEE Trans. Electron Devices* **65**, 2287 (2018).
- [46] H. F. Talbot, Facts relating to optical science No. IV, *London, Edinb. Philos. Mag. J. Sci.* **9**, 401 (1836).
- [47] L. A. Rivlin and V. S. Shil'dyaev, Polyharmonic waveguide for coherent light, *Radiophys. Quantum Electron.* **11**, 318 (1968).
- [48] G. G. Denisov, D. A. Lukovnikov, and M. Yu. Shmelyov, in *Digest of 18 Int. Conf. on IR and MM Waves*, Colchester, UK (1993), p. 485.
- [49] S. V. Kuzikov, Wavebeam multiplication phenomena to RF power distribution systems of high-energy linear accelerators, *Int. J. Infrared Millimeter Waves* **19**, 1523 (1998).
- [50] H. S. Marks and A. Gover, Talbot effect mm-wave resonator for an electrostatic accelerator free electron laser, *IEEE Trans. Microw. Theory Tech.* **66**, 3 (2018).
- [51] H. A. Haus, Mode-locking of lasers, *IEEE J. Sel. Top. Quantum Electron.* **6**, 1173 (2000).
- [52] C. Pellegrini, A. Marinelli, and S. Reichel, The physics of x-ray free-electron lasers, *Rev. Mod. Phys.* **88**, 015006 (2016).
- [53] Y. Y. Danilov, M. I. Petelin, and S. Tantawi, A Coaxial 2D-Periodic perforated directional coupler, *Radiophys. Quantum Electron.* **54**, 731 (2012).
- [54] G. G. Denisov, V. L. Bratman, A. W. Cross, W. He, A. D. R. Phelps, K. Ronald, S. V. Samsonov, and C. G. Whyte, Gyrotron Traveling Wave Amplifier with a Helical Interaction Waveguide, *Phys. Rev. Lett.* **81**, 5680 (1998).
- [55] A. V. Savilov, Account of the feedback frequency dispersion in spatio-temporal equations of a free-electron laser, *Opt. Commun.* **123**, 133 (1996).
- [56] Ya. L. Bogomolov, V. L. Bratman, N. S. Ginzburg, M. I. Petelin, and A. D. Yunakovskiy, Nonstationary generation in free electron lasers, *Opt. Commun.* **36**, 209 (1981).
- [57] T. M. Antonsen, Jr. and B. Levush, Mode competition and suppression in free electron laser oscillators, *Phys. Fluids B* **1**, 1097 (1989).
- [58] V. L. Bratman and A. V. Savilov, Competition of longitudinal modes and the scenario of single-mode regime build-up for the FOM-Fusion-FEM project, *Nucl. Inst. Methods Phys. Res. A* **358**, 182 (1995).
- [59] P. V. Logachev, G. I. Kuznetsov, A. A. Korepanov, A. V. Akimov, S. V. Shiyankov, O. A. Pavlov, D. A. Starostenko, and G. A. Fat'Kin, LIU-2 linear induction accelerator, *Instrum. Exp. Tech.* **56**, 672 (2013).
- [60] A. Akimov, P. Bak, P. Logachev, O. Nikitin, in *Digest of Technical Papers-IEEE International Pulsed Power Conference*, vol. 2015, art. no. 7296931 (2015).
- [61] N. S. Ginzburg and N. Y. Peskov, Nonlinear theory of a free electron laser with a helical wiggler and an axial guide magnetic field, *Phys. Rev. Spec. Top.-Accel. Beams* **16**, 090701 (2013).
- [62] L. A. Vainstein, *Electromagnetic Waves* (Radio i Sviaz, Moscow, 1988), 2nd ed.